Int. J. Electrochem. Sci., 17 **(2022)** Article Number: 220239, doi: 10.20964/2022.02.05

International Journal of
ELECTROCHEMICAL
SCIENCE
www.electrochemsci.org

Comparative Analysis of Corrosion Resistance of 20# and L245NS Steels in the CO_2-saturated Simulated Oilfield Solution with Trace Amounts of H_2S

Z.F. Yin [1,2,], B. Ma [3], F. Wang[4], Z.Y. Cheng[1]*

[1] School of Mechanical and Material Engineering, Xi'an University, Xi'an 710065, P R China
[2] Shaanxi Key Laboratory of Surface Engineering and Remanufacturing, Xi'an 710065, P R China
[3] Research Institute of Shaanxi Yanchang Petroleum (Group) Co. LTD, Xi'an 710065, P R China
[4] Jingbian Oil Production Plant, Yanchang Oilfield Co. Ltd, Yulin 718500, P R China
[*]E-mail: yinzhifu919@sohu.com

Received: 13 October 2021 / *Accepted:* 28 November 2021 / *Published:* 5 January 2022

The study of the electrochemical corrosion behavior on both 20# and L245NS steels were conducted in CO_2-saturated simulated oilfield solution with trace amounts of H_2S at 25ºC and 45ºC by potentiodynamic polarization curve, EIS and SEM medthods. The corrosion parameters of measured Nyquist plots fitted by ZView software were theoretically analyzed and discussed. The results indicated that the corrosion potential (E_{corr}) became more negative and that the corrosion current density (i_{corr}) decreased with the addition of 0.1*wt*.% $Na_2S{\cdot}9H_2O$. At 45ºC, the Warburg impedance characteristics of diffusion process appeared whereas a depressed capacitive semi-circle at 25ºC in a low frequency region was observed for 20# and L245NS steels in the low sulfur-containing condition. Trace amounts of H_2S can lead to the degradation effect on carbon steel, and L245NS steel has relatively better resistance performance than 20# steel to sulfur-containing corrosive solution.

Keywords: 20# steel; L245NS steel; H_2S/CO_2 corrosion; polarization curve; EIS

1. INTRODUCTION

Some oilfield reservoir contain very small amounts of sulfur-containing substances or because of long-term water injection in the pipeline breeding a large number of sulfate reduction bacteria (SRB), will eventually form in the pipeline containing H_2S, HS^- and other sulfur-containing media corrosion environment, oil fields are often accompanied by a certain amount of CO_2 gas, the ground pipeline and metal facilities will produce different degree of corrosion. [1,2]. Corrosion behavior and mechanism of pipeline materials in the H_2S- and CO_2- containing oilfield condition were influenced by many important

factors such as temperature, H_2S partial pressure, CO_2 partial pressure, flow velocity, corrosion product, water percent, chemical composition of produced water, material organization and chemical composition. Carbon steels possessed the reliable mechanical properties and low-cost economy in oil and gas production industry, but they were extremely susceptible to sweet corrosion (only CO_2) and sour (CO_2+H_2S) corrosion environment [3,4].

Under CO_2 and H_2S corrosion condition, some views suggested that the direct hydration of H_2S was the dominant cathodic reaction step, and the dominant cathodic reactions including the reduction of H^+ and H_2S would play a buffering role on H_2S corrosion mechanism [5,6]. It was also well proposed that H_2S might play a dual effect in CO_2 and H_2S co-existing corrosion system, while trace amounts of the instantaneous formation of corrosion product layer of iron sulfide could decrease corrosion rate due to inhibition effect, higher concentration could increase the rate of corrosion due to acceleration effect [7,8]. Ma *et al*. thought that H_2S could play an acceleration effect on both the anodic iron dissolution and the cathodic hydrogen evolution except for certain special condition where the lower H_2S concentrations and the longer immersion times were met simultaneously [9].

In oilfield environment with the coexisting H_2S and CO_2, the electrochemical corrosion of pipeline or equipment occurred, and hydrogen brittle phenomena such as sulphide stress corrosion cracking and hydrogen induced cracking occurred, and in severe cases even it could lead to production safety accidents such as pipeline breakage. Pipeline steel in an oil and gas environment containing H_2S and CO_2, hydrogen produced by H_2S dissocation and H_2CO_3 corrosion could enter into the steel and gathered in non-metallic debris and partialization belt, which would form a bubble that cracked and increased the service risk of the pipeline [10,11].

Although lots of researches related to H_2S/CO_2 corrosion in the past several decades were carried out, the viewpoints in these literatures were somewhat confusing and seemingly inconsistent which were attributed to the complexity of H_2S/CO_2 corrosion oilfield environment. The chemistry mechanism related with the dissolved hydrogen sulfide was very complex and seemingly minor change in experimental conditions could often lead to dramatically different results. The common method in indoor experiments for evaluating metallic pipeline materials subjecting to H_2S/CO_2 corrosion under condition of stress was carried out in NACE TM 0177 solution (CH_3COOH, CH_3COONa, NaCl, pH 3.5, with and without the saturation of H_2S) [12]. However, rarely available literatures related to the corrosion mechanism of carbon steel were discussed in the presence of HAc, chlorides, CO_2 and H_2S [13]. In addition, some researches of H_2S/CO_2 corrosion were focused on low carbon steels or stainless steels [14-16], but little consideration on anti-sulfur pipeline steel such as L245NS steel. The work was to carry out one comparative investigation on the corrosion behavior between common 20# and anti-sulfur L245NS pipeline steels by the methods of potentiodynamic polarization sweep, electrochemical impedance spectroscopy (EIS) and scanning electron microscopy (SEM) with EDS in CO_2-saturated simulated oilfield solution containing 3.5*wt*.%NaCl and 0.5*wt*.%CH_3COONa with and without the addition of 0.1*wt*.% $Na_2S{\cdot}9H_2O$ at 25°C and 45°C, where $Na_2S{\cdot}9H_2O$ could turn into H_2S_{aq} HS^- and S^{2-} species in the acid solution.

2. EXPERIMENTAL METHOD

2.1. Experimental preparation

All specimens machined from 20# and L245NS steels with the chemical compositions (*wt.*%) were shown in Table 1. The specimens were processed into cylinder with *Φ*15 mm×5 mm dimension, which were embedded in epoxy resin with one exposed working copper wire. Before the electrochemical tests, the specimen surfaces were progressively wet-ground with SiC sand papers from 600 to 1200 grits, then rinsed with absolute alcohol and with deionized water. One new specimen was always used for each experiment.

Table 1. Chemical compositions of specimens of 20# and L245NS steels

Material	Element contents（*wt.*%）									
	C	Si	Mn	P	S	Cr	Ni	Mo	Ti	Cu
20#	0.20	0.32	0.60	0.015	0.012	0.03	0.02	-	-	0.04
L245NS	0.10	0.24	1.18	0.012	0.003	0.056	0.026	0.022	0.02	-

The experimental base electrolyte solution with 3.5*wt.*%NaCl and 0.5*wt.*%CH_3COONa were prepared using analytical grade reagents and deionized water. The low sulfur-containing electrolyte solution was introduced by adding 0.1*wt.*% $Na_2S·9H_2O$ since it would turn into H_2S_{aq}, HS^- and S^{2-} species in acidic solution saturated CO_2 in order to simulate the oilfield acid corrosion environments with coexisting H_2S and CO_2. In addition, CH_3COONa could also turn into CH_3COOH and CH_3COO^-. The electrolyte solutions were firstly deaerated by purging with N_2, and then by bubbling with CO_2 respectively for 30 min to one stable CO_2-saturated state prior to the electrochemical tests.

2.2. Electrochemical measurement

The electrochemical tests were conducted by potentiodynamic polarization sweep and electrochemical impedance spectroscopy (EIS) methods in a conventional three-electrode cell of Ametek Princeton PARSTAT 4000A+. The working electrodes were respectively 20# and L245NS specimens, the counter electrode was a pair of graphites and the reference electrode a saturated calomel electrode (SCE). The potentiodynamic polarization curves were measured by sweeping the potential from -0.25 V vs. open circuit potential (OCP) to 0.1 V vs. SCE at a scan rate of 0.25 mV/s.

The EIS measurements were carried out at OCP by applying sinusoidal 10 mV amplitude perturbation and one frequency range from 100 kHz to 10 mHz. All potentials were measured with respect to SCE. Each experiment was conducted at least two times for better reproducibility. Prior to the EIS measurement, an open circuit potential was conducted until the potential was stable. The EIS data were fitted by equivalent circuit models of ZView software. All experimental temperatures were respectively controlled at 25ºC and 45ºC.

2.3. Corrosion product layer analysis

The surface morphologies and chemical compositions of corrosion product layers on 20# and L245NS steels were analyzed by using the JSM-6610LV scanning electron microscopy (SEM) equipped with energy dispersive spectroscopy (EDS).

3. RESULTS AND DISCUSSION

3.1. Potentiodynamic polarization curves

3.1.1. Measurement at 25°C

Figure 1 shows the potentiodynamic polarization curves of both 20# and L245NS steels obtained in CO_2-satruated simulated oilfield solution with and without 0.1*wt*.% $Na_2S{\cdot}9H_2O$ at 25°C. The cathodic branch curve shifts to the decreasing direction of the current density with the addition of 0.1*wt*.% $Na_2S{\cdot}9H_2O$. There is no various limiting cathodic current region which can be seen in the cathodic branch curves besides the curve 3 of L245NS steel in Fig. 1b. At the more negative potential in the cathodic branch curves, only the weak charge transfer impact characterization by direct H_2O reduction was observed. The anodic branch curves have similar characteristics with or without the exist of H_2S_{aq} and HS^- species, and only one small turning peak of the anodic branches of polarization curve 3 is observed around -0.6 V for L245NS steel in Fig. 1b, which is probably related to the instantaneous adsorption of $OH^-_{(aq)}$, $HCO_3^-{}_{(aq)}$, $CH_3COO^-{}_{(aq)}$ and $HS^-_{(aq)}$ forming intermediates with steel substrate.

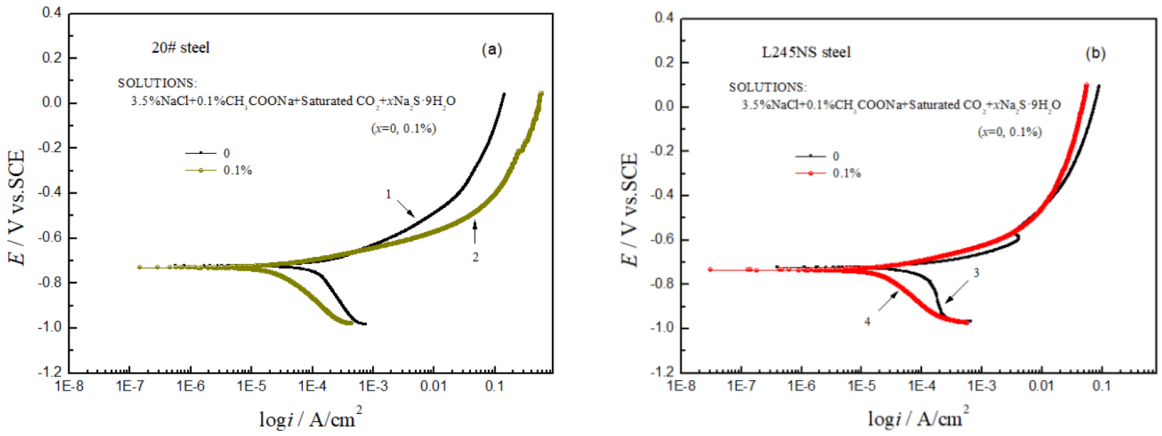

Figure 1. Polarization curves of 20# and L245NS steels obtained at 25°C in low sulfur-containing oilfield environment

The corresponding corrosion parameters of the polarization curves of 20# and L245NS steels at 25°C are listed in Table 2. It can be seen that the corrosion potential (E_{corr}) of 20# and L245NS steels becomes slightly negative with the addition of 0.1*wt*.% $Na_2S{\cdot}9H_2O$. The corrosion current density (i_{corr}) of 20# and L245NS steels greatly decreases as the addition of 0.1*wt*.% $Na_2S{\cdot}9H_2O$. It indicates that the trace amounts of H_2S can play a degradation effect on carbon steel, which is in agreement with the results from research by Veloz, *et al.* [17], while it disagrees with the results by Ma *et al.* [18]. Because HS^-

species can strongly chemisorb on metal surface and can displace the adsorbed OH^- species and can react with the metal substrate, and the formed corrosion product Fe_xS_y has good compact density and binding force, which can slow down the dissolution rates of carbon steels. In addition, the anti-sulfur L245NS steel has lower corrosion rates (*i.e.*, i_{corr} values) compared with the ones of the common 20# steel. In the low H_2S-containing case, the cathodic Tafel slopes (β_c) of two pipeline steels decrease for about one half in Table 2, which are extremely dependent on the H_2S_{aq} and HS^- concentrations. The fact is that these β_c values are greater than those β_a values, indicating that the complex nature of the H_2S/CO_2 corrosion processes is mainly controlled by cathodic reactions.

Table 2. Corrosion parameters of the polarization curves obtained on 20# and L245NS steels at 25°C

Parameter	20# steel		L245NS steel	
	free $Na_2S·9H_2O$	0.1% $Na_2S·9H_2O$	free $Na_2S·9H_2O$	0.1% $Na_2S·9H_2O$
E_{corr}/mV	-722	-730	-723	-735
i_{corr}/μA	140.4	35.2	121.5	33.8
β_a/mV·dec^{-1}	141	66	80	84
β_c/mV·dec^{-1}	-448.	-299	-673	-302

3.1.2. Measurement at 45°C

The corrosion behavior of the polarization curves obtained on 20# and L245NS steels with and without 0.1*wt*.% $Na_2S·9H_2O$ at 45°C are shown in Fig. 2. It showed that the similar corrosion characteristics in the anodic branch curves. There are some small differences among the characteristics of cathodic branch curves with introduction of 0.1*wt*.% $Na_2S·9H_2O$ chemical agent at 45°C. The limiting cathodic current region can be only observed on 20# steel for curve 1 in free $Na_2S·9H_2O$ case in Fig. 2a. For the polarization curves, there is no strong sensitivity on the corrosion behaviors of 20# and L245NS steels at 45°C with respect to those at 25°C.

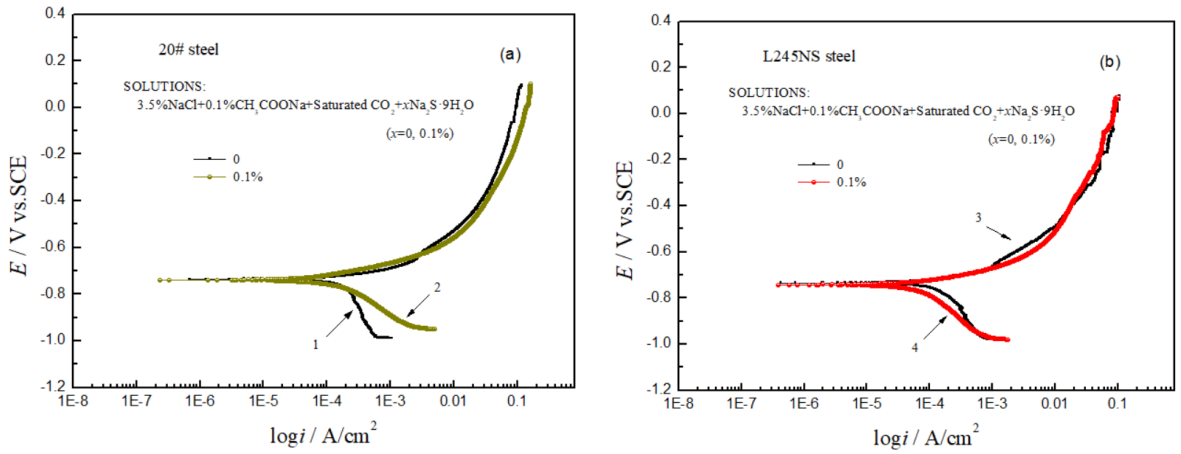

Figure 2. Polarization curves of 20# and L245NS steels obtained at 45°C in low sulfur-containing oilfield environment

In Table 3, the corresponding corrosion parameters of the polarization curves obtained at 45ºC in low sulfur-containing oilfield environment can provide more information for the H_2S/CO_2 corrosion process. The E_{corr} values become slightly more negative with the introduction of 0.1*wt*.% $Na_2S{\cdot}9H_2O$, and there are little difference between the E_{corr} values of 20# and L245NS steels. The i_{corr} value of 20# and L245NS steel decrease for the case of 0.1*wt*.% $Na_2S{\cdot}9H_2O$, indicating the corrosion rate of L245NS steel decreases under the degradation effect of H_2S_{aq} and HS^- species. As compared to the i_{corr} values at 25ºC in Table 2, the corresponding i_{corr} values at 45ºC in Table 3 significantly increase at the same condition, which indicates that the temperature factor has one extremely important influence on corrosion behavior of carbon steel in low sulfur-containing oilfield environment.

Table 3. Corrosion parameters of the polarization curves of 20# and L245NS steels obtained at 45ºC

Parameter	20# steel		L245NS steel	
	free $Na_2S{\cdot}9H_2O$	0.1% $Na_2S{\cdot}9H_2O$	free $Na_2S{\cdot}9H_2O$	0.1% $Na_2S{\cdot}9H_2O$
E_{corr}/mV	-736	-741	-735	-744
i_{corr}/μA·cm^{-1}	224.4	154.5	192.8	130.5
β_a/mV·dec^{-1}	97	97	109	98
β_c/mV·dec^{-1}	-353	-213	-344	-260

According to the my previous papers by Z.F. Yin, which are related to the similar electrochemical tests on low-alloy steel 3Cr, anti-sulfur steels of 80Sand 110S in similar CO_2/H_2S testing conditions [14,19]. For the free and 0.1% $Na_2S{\cdot}9H_2O$ cases, at 25ºC and 45ºC, the i_{corr} values of 3Cr steel were smaller than the ones of 20# steel and L245NS steel, but the change trend was consistent, *i.e.*, the i_{corr} values decreases with the addition of 0.1% $Na_2S{\cdot}9H_2O$, and the i_{corr} values increase when temperature from 25ºC to 45ºC. However, Ma *et al.* considered that the presence of H_2S can accelerate anodic and cathodic processes which take place on the metal surface [20]. And a study from Yan *et al.* [21], they considering the effect of chlorides on anodic dissolution of iron in an acid medium of $HAc/Ac^-/Cl^-$ after adding H_2S with H_2S, it showed the absence of corrosion products on the iron surface probably due to the capacity of chloride to prevent the formation of sulfides due to their competitive adsorption with HS^-, diminishing the anodic process acceleration.

It can be seen that the main compositional differences between 20# and L245NS steels are the Mn, Cr, Ti and Mo elements contents as listed in Table 1. However, the alloy elements contents are very small except for Mn element. Generally, Mn combined with S can form the inclusion of MnS, which serves as microcathode in steel and promotes localized corrosion which plays a negative role on H_2S/CO_2 corrosion. In the meantime, little quantities of Ni, Ti and Mo elements have almost little effect on the corrosion resistance. In Table 1, there are little amounts of the alloy element Mo and Ti in L245NS steel. According to the data of corrosion current densities of polarization curves, L245NS steel has similar resistance as 20# steel probably due to the similar chemical compositions. The anti-sulfur L245NS steel perhaps has more superior performance to the sulphide stress corrosion cracking (SSCC) that needs to be validated by future experiment.

3.2. Electrochemical impedance spectroscopy

3.2.1. Measurement at 25°C

The Nyquist plots of 20# and L245NS steels obtained in low sulfur-containing oilfield environment with and without 0.1*wt*.% $Na_2S{\cdot}9H_2O$ at 25°C are respectively presented in Fig. 3. The research shows the good fitting data by equivalent circuit models shown in Fig. 3c and 3d. The Nyquist plots demonstrate that the shape and size have obvious differences for free and 0.1*wt*.% $Na_2S{\cdot}9H_2O$ cases. For the H_2S-free case, the Nyquist plot has two time constants consisting of one depressed capacitive semicircle at the intermediate frequency, an inductive small reactance semicircle at the low frequency. For the case of 0.1*wt*.% $Na_2S{\cdot}9H_2O$ addition, the corrosion characteristics of Nyquist plot has changed, *i.e.*, the inductive reactance semicircle disappears and capacitive semicircle appears in the low frequency region because metal substrate surfaces are completely covered by corrosion products.

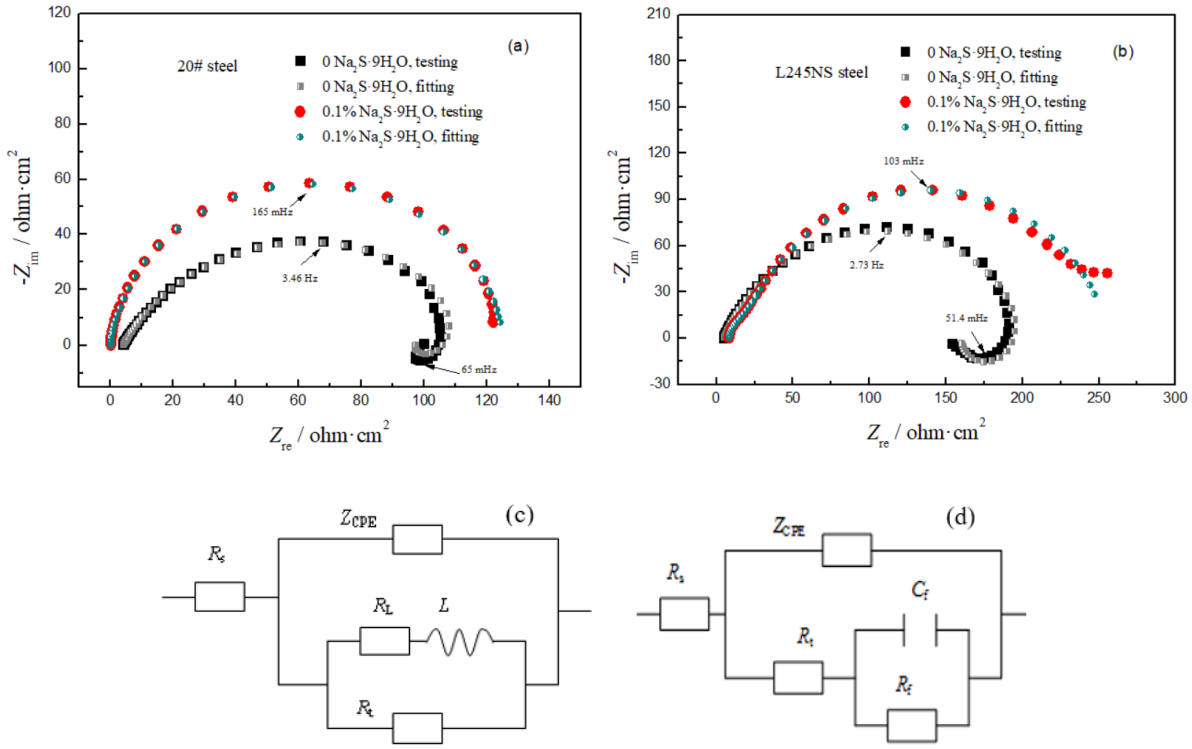

Figure 3. Nyquist plots of 20# and L245NS steels obtained at 25°C in low sulfur-containing oilfield environment. (a) testing; (b) fitting; (c) and (d) equivalent current models

The depressed capacitive semi-circles are probably attributed to three influencing factors including the heterogeneous surface roughness, the non-uniform distribution of current density and the formation of corrosion product layer on metal surface [22]. It is clearly observed that the diameter size of the capacitive semicircle increases with the addition of 0.1*wt*.% $Na_2S{\cdot}9H_2O$, which indicates that the formed corrosion product layer of Fe_xS_y plays a certain good protection for steel substrate. According the research result from Arzola *et al.* [11], the elelctrochemical tests were performed in presence of acetate, which decreased iron sulfide precipitation, and they considered that impedance response was

mainly dominated by anodic reactions.

The fitting parameters of impedance data of 20# and L245NS steels obtained at 25°C are shown in Table 4. For the applied circuit models, R_s is the solution resistance between the working electrode and reference electrode, R_t is the charge transfer resistance, L is the inductance related with the adsorption product, R_L is the inductive resistance of adsorption product, C_f and R_f are the capacitance and resistance of corrosion product layer, respectively. In general, the constant phase element (CPE) represents the impedance of the capacitance element Q, which is widely used as scattered circuit element in equivalent circuits for non-ideal frequency response.

Table 4. Fitting parameters from the Nyquist plots of 20# and L245NS steels by equivalent circuit models at 25°C

Parameter	20# steel		L245NS steel	
	free $Na_2S·9H_2O$	0.1% $Na_2S·9H_2O$	free $Na_2S·9H_2O$	0.1% $Na_2S·9H_2O$
R_s ($\Omega·cm^2$)	4.3	4.2	7.9	8.5
Q-Y_o ($\Omega^{-1}·cm^{-2}·s^n$)	$1.02×10^{-3}$	$5.74×10^{-3}$	$3.60×10^{-4}$	$1.64×10^{-3}$
Q-n_o	0.72	0.98	0.76	0.97
R_t ($\Omega·cm^2$)	93.5	34.5	233.1	25.4
L ($H·cm^2$)	19.2	-	123.9	-
R_L ($\Omega·cm^2$)	25.7	-	76.8	-
Q-Y_f ($\Omega^{-1}·cm^{-2}·s^n$)	-	$3.48×10^{-3}$	-	$4.87×10^{-3}$
Q-n_f	-	0.86	-	0.83
R_f ($\Omega·cm^2$)	-	90.6	-	224.1

In Table 4, at 25°C, the R_t value (93.5 $\Omega·cm^2$) of 20# steel is much smaller than that of L245NS steel (233.1 $\Omega·cm^2$), indicating that L245NS steel has relatively better resistance performance in the H_2S-free case. The L and R_L values of L245NS steel are much larger than those of 20# steel, indicating that the adsorption and desorption by adsorbents (or intermediate products) increases and corrosion products can provide better protection. However, under the low sulfur-containing condition, significant change has taken place on the samples surfaces, when inductive reactance semicircle in the low frequency zone disappears, *i.e.*, the intermediate product can be converted into a corrosion product, and the R_f value of 20# steel (90.6 $\Omega·cm^2$) is much smaller than the R_f value of L245NS steel (224.1 $\Omega·cm^2$). It is shown that L245NS steel also has superior sulfur corrosion resistance compared to 20# steel after adding small amounts of the sulfur-containing $Na_2S·9H_2O$ to the testing solution.

3.2.2. Measurement at 45°C

The Nyquist plots of 20# and L245NS steels obtained in low sulfur-containing oilfield environment with and without 0.1*wt*.% $Na_2S·9H_2O$ at 45°C are respectively presented in Fig. 4. For the H_2S-free case, the Nyquist plot of 20# steel consists of three time constants, *i.e.*, one depressed capacitive

semicircle in the intermediate frequency region, an inductive reactance semicircle and one small capacitive semicircle in the low frequency region at 45ºC, which is similar to the corrosion characteristics of L245NS steel. It shows that intermediate products and protective corrosion products are formed on the samples surfaces at 45ºC. Under the low sulfur-containing condition, the two steels show characteristics of two time constants, namely, the capacitive arc in the intermediate frequency zone and the Warburg impedance diffusion tail in the low frequency zone. Generally, the characteristic at the low frequency is caused by the diffusion impedance of the forming Fe_xS_y corrosion products.

Contrasting with the result from Ayagou et al. [23], the Nyquist plots consisted of a capacitive loop at high frequency interpreted by the charge transfer resistance, followed by a 45º tail at low frequency assumed to represent a diffusion process for the tests in 30 g/L NaCl solutions with various H_2S concentrations ranging from 100 mass ppm to 2550 mass ppm. It is believed that these high values are associated with the rapid formation of a conductive iron sulfide scale.

According to the equivalent circuit models in Fig. 4c and 4d, the corresponding fitting parameters from the Nyquist plots obtained at 45ºC by are listed in Table 5. Where, Z_w is Warburg impedance, other circuit components have the same physical significance. From the dispersion index Q-n_o, the capacitance of the two steels are relatively higher at low sulfur-containing conditions compared to that at the H_2S-free conditions. At the low sulfur-containing conditions, the R_t value of 20# steel (34.7 Ω·cm^2) is smaller than that of L245NS steel (57.8 Ω·cm^2), indicating that L245NS steel at 45ºC has relatively better anti-sulfur resistance performance.

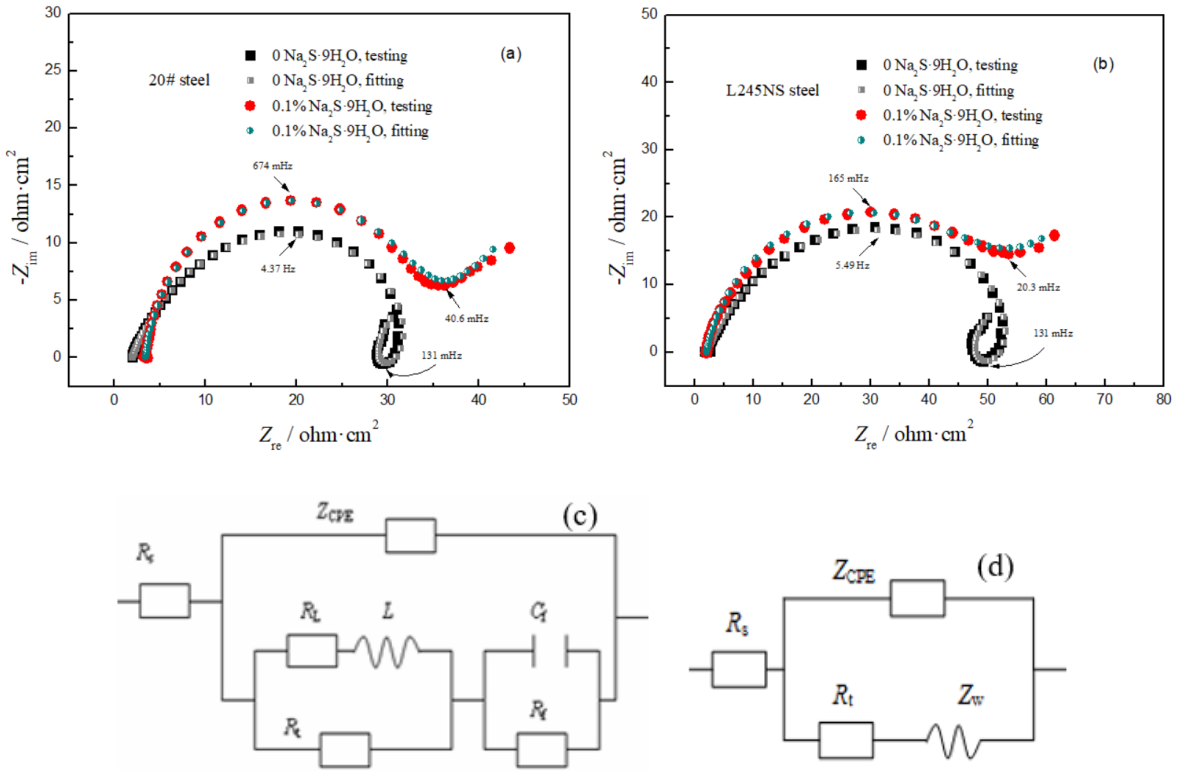

Figure 4. Nyquist plots of 20# and L245NS steels obtained at 25ºC in low sulfur-containing oilfield environment. (a) testing; (b) fitting; (c) and (d) equivalent current models

Table 5. Fitting parameters obtained from the Nyquist plots of 20# and L245NS steels by equivalent circuit models at 45ºC

Parameter	20# steel		L245NS steel	
	free $Na_2S·9H_2O$	0.1% $Na_2S·9H_2O$	free $Na_2S·9H_2O$	0.1% $Na_2S·9H_2O$
R_s ($\Omega·cm^2$)	2.0	3.4	2.2	2.0
Q-Y_o ($\Omega^{-1}·cm^{-2}·s^n$)	$2.56×10^{-3}$	$7.97×10^{-4}$	$1.37×10^{-3}$	$15.28×10^{-3}$
Q-n_o	0.71	0.92	0.72	0.86
L ($H·cm^2$)	64.9	-	136.3	-
R_L ($\Omega·cm^2$)	127.2	-	222.2	-
C_f ($F·cm^{-2}$)	4.1	-	2.5	-
R_f ($\Omega·cm^2$)	9.8	-	14.3	-
R_t ($\Omega·cm^2$)	30.1	34.7	47.6	57.8
Z_w ($\Omega·cm^2$)	-	0.33	-	0.21

The L value and R_L value of L245NS steel are much larger than the corresponding values of 20# steel (nearly twice), indicating that the adsorption by adsorbents (or intermediate products) adsorption galloping effect increased, corrosion products played a better protection.

From the low frequency capacitive resistance without sulfur conditions, the samples surfaces forms a certain corrosion product, but the R_f value is small and the difference between the two steels is very small. Under low sulfur-containing condition, the characteristics of the Nyquist plots were obviously changed, at which inductive reactance characteristics in the low frequency zone disappeared and the mechanism also becomes substance transfer controlling. The samples surfaces form one layer of well-protected corrosion products, which differs from the Z_w values.

According to the my previous papers by Z.F. Yin, which are related to the similar EIS tests on low-alloy steel of 3Cr, anti-sulfur steels of 80Sand 110S in similar CO_2/H_2S testing conditions [14,19]. In the past researches, the Nyquist plots have similar characterization at 45ºC in the free and 0.1% $Na_2S·9H_2O$ cases, but at 25ºC, there is no characterization of the Warburg impedance diffusion tail on in the low frequency zone in the 0.1% $Na_2S·9H_2O$ case. It can be seen that the results on 20# and L245NS steel were well consistent in the similar temperature and sulfur-containing conditions.

In addition, at 25ºC or 45ºC, the R_t values of 20#and L245NS steel have similar change trend to 3Cr *i.e.* decreasing with the addition of 0.1% $Na_2S·9H_2O$, but identical results for the anti-sulfur steels of 80S and 110S, it can be considered that one layer of protective corrosion products rapidly formed on 80S and 110S.

3.3. Analysis of corrosion product layers

Figure 5 and Figure 6 show the microscopic surface morphologies and X-ray diffraction energy spectra of corrosion product layers on samples respectively at 25ºC and 45ºC in 0.1*wt*.% $Na_2S·9H_2O$ case. In the low sulfur-containing environment, the forming corrosion products are porous and loose at 25ºC, whereas at 45ºC, the corrosion products are relatively thick and loose, and in some micro-area

where corrosion cracks has occurred as shown in Fig. 6b, the corrosive species such as Cl^-, $H_2CO_{3(aq)}$, HCO_3^- and $H_2S_{(aq)}$, HS^- can readily pass through the cracked corrosion product layer and then reach the layer/substrate interface, where further electrochemical reactions occur, then resulting in more severe localized corrosion.

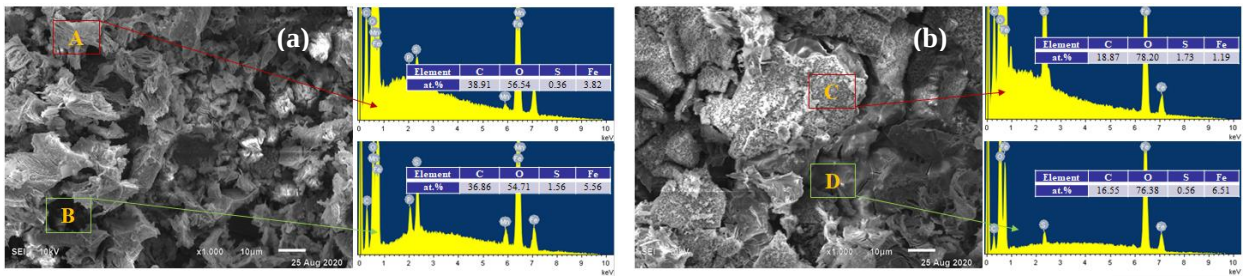

Figure 5. SEM and EDS analysis of corrosion product layers on samples at 0.1*wt.*% $Na_2S{\cdot}9H_2O$ conditions at 25ºC. (a) 20#; (b) L245NS

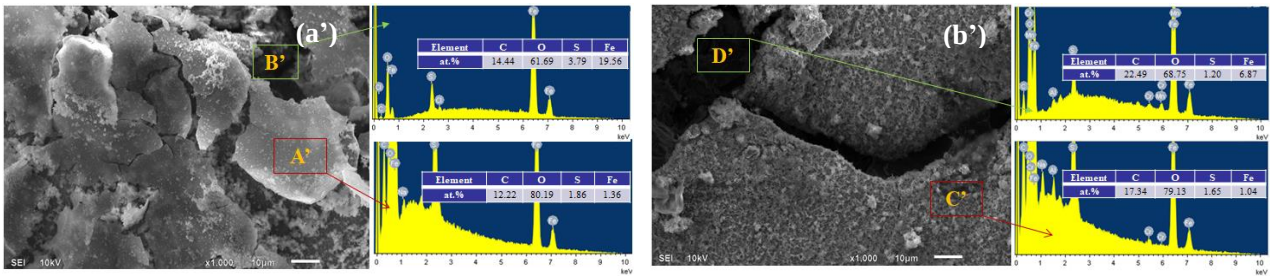

Figure 6. SEM and EDS analysis of corrosion product layers on samples at 0.1*wt.*% $Na_2S{\cdot}9H_2O$ conditions at 45ºC. (a) 20#; (b) L245NS

The EDS analysis are carried out on each corrosion sample at the accelerating voltage of 10 mV which can lead to X- ray penetrates the corrosion product layer into the steel matrix, therefore the element contents are not very accurate and only act as contrast and reference at various test conditions. The corrosion products mainly contain elements C, O, S and Fe, which are probably a mixture of iron carbonate, iron sulfides, and iron oxides due to the multiple reactants. At 25ºC, it can be seen that the content of S element are 0.36*at.*% and 1.56*at.*% in corrosion products at A and B zones of 20# steel, 1.73*at.*% and 0.56*at.*% in corrosion products at C and D zones of L245NS steel. At 45ºC, it can be seen that the content of S element are 1.86*at.*% and 3.79*at.*% in corrosion products at A' and B' zones of 20# steel, 1.65*at.*% and 1.20*at.*% in corrosion products at C' and D' zones of L245NS steel. It needs to be pointed out that A, A', C, C' are the "first deposition" corrosion product crystals and B, B', D, D' are the "second deposition" corrosion product crystals. It can be found that the "second deposition" corrosion product crystals of 20# steel have more S contents, whereas for L245NS steel, the results are contrary at 25ºC or 45ºC, which indicating that L245NS steel has relative superior performance for the low sulfur-containing condition. However, because the trace amounts of $Na_2S{\cdot}9H_2O$ is added, the whole corrosion process is mainly controlled by CO_2 corrosion instead of H_2S corrosion, it is very difficult to judge the corrosion resistance difference between 20# and L245NS based on a small amount of S content. But it can be found that the S content at 45ºC is much higher than that at 25ºC.

According to the previous literatures researches [16,24], all kinds of polymorphs of iron sulfide can form acted as corrosion products on mild steel in H_2S-containing corrosion system, including amorphous ferrous sulfide (FeS), mackinawite (FeS), cubic ferrous sulfide (FeS), troilite (FeS), pyrrhotites ($Fe_{1-x}S$), smythite ($Fe_{3+x}S_4$), greigite (Fe_3S_4), pyrite (FeS_2) and marcasite (FeS_2). The concentration of sulfide ion increases with immersion time, and form sulfur-richer pyrrhotite. Meanwhile, the particles become more uniform and dense [16].

In this work, the result from EDS spectra shows that the corrosion products contain most of siderite ($FeCO_3$) and some probably polymorphs of iron sulfide such as mackinawite (FeS) or pyrrhotites ($Fe_{1-x}S$) based on the Fe:S ratios and that the C:O ratios as the addition of $Na_2S{\cdot}9H_2O$ concentration.

4. CONCLUSIONS

Corrosion potential of 20# and L245NS steels became slightly more negative and corrosion current density greatly decreased with the addition of 0.1*wt*.% $Na_2S{\cdot}9H_2O$. Compared to the i_{corr} values at 25ºC, the corresponding i_{corr} values at 45ºC significantly increase at the same condition.

For the case of 0.1*wt*.% $Na_2S{\cdot}9H_2O$ addition, the inductive reactance semicircle disappeared and capacitive semicircle appeared in the low frequency region at 25ºC, but Nyqusit plots showed two time constants characteristics including the capacitive arc at the intermediate frequency and the Warburg impedance diffusion tail at the low frequency at 45ºC.

The R_t values of 20# steel were much smaller than those of L245NS steel. The L and R_L values of L245NS steel were much larger than the corresponding values of 20# steel. There were the characterization of “first deposition” and “second deposition” in corrosion product layers.

Trace amounts of H_2S would lead to the degradation effect on carbon steel. The corrosion processes was mainly controlled by cathodic reactions. L245NS steel has relatively better resistance performance than 20# steel.

ACKNOLEDGMENTS
The authors kindly thank the support from Shaanxi Education Department Science and Technology Research Plan (21JS035) and Xi'an Science and Technology Plan (2020KJWL01).

References

1. F.X. Shi, L. Zhang, J.W. Yang, M.X. Lu, J.H. Ding, and H. Li, *Corros. Sci.*, 102 (2016) 103.
2. M.A. Mohtadi-Bonab, M. Eskandari, K.M.M. Rahman, and R. Ouellet, Int. *J. Hydrogen. Energ.*, 41 (2016) 4185.
3. D.P. Li, L. Zhang, J.W. Yang, and M.X. Lu, *Int. J. Min. Met. Mater.*, 21 (2014) 388.
4. J. Bana’s, U. Lelek-Borkowska, B. Mazurkiewicz, and W. Solarski, *Electrochim. Acta*, 52 (2007) 5704.
5. A. Kahyarian, and S. Nesic, *Electrochim. Acta*, 297 (2019) 676.
6. C. Sun, J. Sun, Y. Wang, X. Lin, X. Li, X. Chen, and H. Liu, *Corros. Sci.*, 107 (2016) 193–203.
7. Z.Q. Bai, Z.F. Yin, D. Wei, X.F. Wang, and C.X. Yin, *Mater. Corros.*, 61 (2010) 689.
8. X.L. Cheng, H.Y. Ma, J.P. Zhang, X. Chen, S. H. Chen, and H. Q. Yang, *Corrosion*, 54 (1998) 369.

9. H.Y. Ma, X.L. Cheng, G.Q. Li, S.H. Chen, Z.L. Quan, S.Y. Zhao, and L. Niu, *Corrosion*, 54 (1998) 634.
10. M.E. Orazem, and B. Tribollet, Electrochemical impedance spectroscopy, *Wiley ed.*, in: The Electrochemical Society Series (second ed.), 2017.
11. S. Arzola, and J. Genesca, *J. Solid State Electrochem.*, 9 (2005) 197.
12. Standard Technical Method, NACE TM 01 77, *NACE*, 1996.
13. M.M. Singh, and A. Gupta, *Corrosion*, 56 (2000) 371.
14. Z.F. Yin, Y.L. Zhang, G.R. Chang and T.Q. Yang, *J. Mater. Eng. Perform.*, 29 (2020) 5442.
15. G.E. Li. B.S. Huang, S.S. Zhang, X. Wen and T.N. Li. *Int. J. Electrochem. Sci.*, 15 (2020) 121.
16. H.Y. Wang, C. Yu, X.H. Gao, L.X. Du and H.W. Wang, Int. J. Electrochem. Sci., 15 (2020) 6737.
17. M.A. Veloz, and I. Gonzalez, *Electrochimica Acta*, 48 (2002) 135.
18. H.Y. Ma, X.L. Cheng, G.Q. Li, S.H. Chen, Z.L. Quan, S.Y. Zhao, and L. Niu, *Corros. Sci.*, 42 (2000) 1669.
19. Z.F. Yin, L. Liu, Y. Wang, T.Q. Yang and Y.X. Chen, *Int. J. Electrochem. Sci.*, 15 (2020) 10825.
20. H. Ma, X. Cheng, G. Li, S. Chen, Z. Quan, S. Zhao, L. Niu, *Corros. Sci.*, 42 (2000) 1669.
21. L.J. Yan, L. Niu, H.C. Lin, W.T. Wu, S.Z. Liu, *Corros. Sci.*, 41 (1999) 2303.
22. E. McCafferty, *Corros. Sci.*, 39 (1997) 243.
23. M.D.D. Ayagou, T.T.M. Tran, B.T.J. Kittel, E. Sutter, N. Ferrando, C. Mendibide , C. D. Thual. *Electrochim. Acta*, 5282 (2018) 775e783.
24. W. Sun, S. Nesic, and D. Young, *Ind. Eng. Chem. Res.*, 47 (2008) 1738.